Journal of Inflammation Research

Dovepress
open access to scientific and medical research

Open Access Full Text Article

ORIGINAL RESEARCH

An Experimental Animal Study: Electroacupuncture Facilitates Antiviral Immunity Against Hepatitis B Virus Through the IFN-γ/JAK/STAT Axis

Yan Yang[1,*], Feilin Ge[2,*], Chen Luo[1], Cai Liao[1], Junyuan Deng[1], Yunhao Yang[1], Yang Chen[1], Xiao Guo[1], Zhaofang Bai[3], Xiaohe Xiao[3], Chenglin Tang[1]

[1]College of Traditional Chinese Medicine, Chongqing Medical University, Chongqing, 400010, People's Republic of China; [2]Department of Chinese Medicine, The First Affiliated Hospital of Zhengzhou University, Zhengzhou, 450052, People's Republic of China; [3]Senior Department of Hepatology, the Fifth Medical Center of Chinese PLA General Hospital, Beijing, 100039, People's Republic of China

*These authors contributed equally to this work

Correspondence: Xiaohe Xiao, Senior Department of Hepatology, The Fifth Medical Center of Chinese PLA General Hospital, Beijing, People's Republic of China, Email pharmacy302xxh@126.com; Chenglin Tang, College of Traditional Chinese Medicine, Chongqing Medical University, Chongqing, People's Republic of China, Email tangchenglin@cqmu.edu.cn

Background: Chronic hepatitis B (CHB) remains a global health challenge, necessitating innovative therapeutic strategies. Enhancing the body's immune response against the hepatitis B virus (HBV) emerges as a fundamental strategy for achieving a functional cure. While acupuncture has shown potential in immune modulation, its specific anti-HBV effects are not well understood. This study evaluates the potential of electroacupuncture (EA) in HBV infection and explores its underlying immunological mechanisms using a mouse model.

Methods: HBV-infected mice were established using the high-pressure hydrodynamic method and divided into four groups: normal saline (NS), EA, sham EA (SE), and tenofovir disoproxil fumarate (TF), with n = 6 per group. During treatment, blood was collected every Sunday via the orbital sinus to monitor HBV DNA, HBsAg, and HBeAg levels. Transcriptomics and metabolomics analyses were employed to unearth clues regarding EA's anti-HBV mechanism. Validation of these mechanisms included splenic T-cell flow analysis, Western blotting, RT-qPCR, immunofluorescence, and ELISA.

Results: Serum HBV DNA levels decreased by 1.10, 0.19, and 1.98 $\log_{10}$ IU/mL in the EA, SE, and TF-treated mice, respectively, compared to the NS. Concurrently, the hepatic HBV DNA levels decreased by 1.09, 0.24, and 2.03 $\log_{10}$ IU/mL. EA also demonstrated superior inhibition of HBV antigens, with serum HBeAg levels decreasing by 43.86%, 8.74%, and 8.03%, and serum HBsAg levels decreasing by 28.01%, 0.26%, and 9.39% in the EA, SE, and TF groups, respectively. Further analysis through transcriptomics and metabolomics revealed that EA's anti-HBV effects primarily hinge on immune modulation, particularly the IFN-γ/JAK/STAT pathway and taurine metabolism. EA also increased the ratio of splenic $CD8^+$ $CD69^+$ and $CD8^+$ IFN-γ^+ T-cells while upregulating key proteins in the JAK/STAT pathway and cytokines associated with antiviral immunity.

Conclusion: EA manifests inhibitory effects on HBV, particularly in antigen suppression, with its mode of action intricately linked to the regulation of IFN-γ/JAK/STAT.

Keywords: hepatitis B virus, electroacupuncture, antiviral activity, immune modulation, IFN-γ

Introduction

Hepatitis B virus (HBV) can persist, leading to chronic necrotizing inflammatory liver disease.[1] Currently, approximately 296 million people worldwide (about 3.7% of the population) are chronic HBV (CHB) carriers, predisposing them to various severe liver diseases, including cirrhosis, liver failure, and hepatocellular carcinoma.[2–4] In 2019, HBV-related diseases resulted in 7.2 deaths per 100,000 people globally.[5] The ideal therapeutic goal for CHB is to achieve functional cure (clinical cure), characterized by sustained undetectable serum HBsAg and HBV DNA, along with negative HBeAg

Received: 5 July 2024
Accepted: 13 September 2024
Published: 19 September 2024

status, with or without HBsAg seroconversion, remission of hepatic inflammation, histopathological amelioration, and a substantial abatement in end-stage liver disease incidence post-effective therapeutic intervention.[6] Although existing antiviral drugs, including nucleos(t)ide analogues (NAs) and pegylated alpha-interferon (PEG-IFN-α), effectively inhibit viral replication, their efficacy in antigenic suppression is limited.[7] A real-world cohort study presented at the annual meeting of the American Association for the Study of Liver Diseases in 2021, based on data from 25 centers across 10 nations/regions, revealed that the 8-year cumulative HBsAg clearance rate among CHB patients treated with ETV/TDF was approximately 1%,[8] a pivotal yardstick denoting function cure.[9] Presently, the achievement of functional cure remains elusive for most patients, emphasizing the urgent need for novel therapeutic modalities to optimize and enhance existing antiviral regimens, thereby bolstering the functional cure rate of CHB.

CHB is characterized as an immune-mediated disease, wherein the HBV exerts its detrimental effects not directly on the liver but through an aberrant immune cascade. The interaction between HBV and the host's immune response plays a crucial role in determining the clinical course, affecting both the regression and progression of the disease. In cases of acute hepatitis B, the body mounts a robust antiviral immune response, significantly influencing viral clearance. In contrast, CHB infection is marked by reduced host immune responsiveness, accompanied by HBV DNA integration within hepatocytes, persistence of HBV cccDNA, T-cell dysfunction, and inadequate B-cell reactivity, collectively hindering HBV eradication.[10,11] Therefore, achieving a cure for CHB necessitates not only direct antiviral modalities but also revitalizing the body's immunity to mount effective innate and adaptive antiviral defenses.[12–14]

Physical therapy methods are becoming increasingly significant in modern medical treatments, primarily due to their role in altering biochemical substances in the body to regulate pathological states.[15] Similarly, EA functions as a physical therapy modality that can induce biochemical changes, which has been recognized for its ability to modulate the body's immune milieu, potentially serving as an adjunct to existing first-line therapeutic agents and offering a novel strategy for CHB management. Numerous studies have demonstrated acupuncture's capacity to enhance various immune cell populations within the body, including NK cells, NKT cells,[16] $CD4^+$ T lymphocytes,[17] and $CD8^+$ T lymphocyte,[18] as well as various immune effector molecules such as immunoglobulins,[19] IFN-γ,[20] and IL-2.[21] Hence, we hypothesize that acupuncture may have the potential advantage in combating HBV through immunological mechanisms. While clinical studies have shown that acupuncture has synergistic anti-HBV effects when used in combination with other treatments, the specific anti-HBV effects of acupuncture alone and its antiviral mechanisms remain unclear.[22–24] Therefore, this study aims to evaluate whether electroacupuncture (EA) exhibits anti-HBV effects through basic experiments and explore its immune-mediated anti-HBV mechanism for the first time. The goal is to address the limited antigenic inhibitory effect of existing first-line drugs and propose a new therapeutic approach of "NAs+acupuncture" for the clinical treatment of CHB, particularly aiming towards achieving functional cure.

Materials and Methods

Reagents and Antibodies

SYBR Green quantitative real-time polymerase chain reaction (qRT-PCR) Master Mix (Cat No. HY-K0522), and RT Master Mix for qPCR (Cat No. HY-K0510) were supplied by Med Chem Express (Monmouth Junction, NJ, USA). TRIzol reagent (Cat No. 260805) was purchased from Invitrogen (Carlsbad, CA, USA). Fluorescent labeled antibodies including CD3 (100204), CD4 (116012), CD8 (100730), CD69 (10453), IFN-γ (505809), and TNF-α (506305) were supplied from Biolegend (California, USA). ELISA kits for IFN-γ (EK280/3-AW1) and TNF-α (EK282/4-AW1) were purchased from Multi Science (Zhejiang, China). Antibodies against JAK1 (3344), p-JAK1 (74129), JAK2 (3230), p-JAK2 (3776), STAT1 (14995), p-STAT1 (9167), and IRF8 (98344) were sourced from Cell Signaling Technology (Boston, USA), whereas anti-IRF8 (18977-1-AP) was purchased from Proteintech (Wuhan, China). Furthermore, anti-p-JAK1 (YP0154), anti-p-JAK2 (YP0306), and anti-SOCS-1 (YT4362) were provided by ImmunoWay, with anti-β-Tubulin (#T0023) acquired from Affinity Biosciences (Jiangsu, China).

Mouse Model of HBV and Grouping

Male C57BL/6 mice, aged 6–8 weeks and weighing 18–20 g, were procured from the Animal Center of Chongqing Medical University (Animal License No. SYXK (Yu) 2022–0016). The experiment was conducted from November 2023 to December 2023. All mice were fasted overnight and kept in cages under controlled conditions (22 ± 2°C, 12 h light/dark cycle with 50% humidity) in the SPF-level animal facility at Chongqing Medical University. The HBV-infected mouse model was established by injecting 20 μg of pAAV-HBV1.2 hBV plasmid via the tail vein using the high-pressure hydrodynamic method. After 3 days, blood samples were collected from the orbital sinus for monitoring the HBsAg, HBeAg, and HBV DNA.

The HBV-infected mice (n = 24) were randomly assigned to four groups: normal saline (NS, receiving NS), EA (receiving EA and NS), sham EA (SE, receiving SE and NS), and positive control tenofovir disoproxil fumarate (TF, receiving TF at 63 mg kg^{-1} d^{-1}), n = 6. Bilateral "Zusanli" (ST36) and "Ganshu" (BL18) acupoints were selected based on our previous report,[25] and the methods described in Experimental Acupuncture.[26] Adhesive tapes were used to ensure full exposure and sterilization,[27] followed by the insertion of needles. The stimulation was administered given to two needles inserted into bilateral ST36 and BL18 acupoints on the ipsilateral side using an electrical stimulator (SDZ-II, Suzhou Medical Appliance Factory, Suzhou, Jiangsu Province, China), set at a frequency of 2/15 hz (amplitude-modulated wave) and an intensity of 0.5 mA for 10 minutes daily. The SE group received similar treatment without electrical stimulation. The intervention was administered once daily for three weeks. Upon completion of the intervention, the blood was collected from the orbital sinus, and mice were sacrificed by cervical dislocation for sampling the liver and spleen tissues for laboratory investigation (Figure 1). All procedures followed Animal Ethics Committee guidelines of Chongqing Medical University (Ethics No. IACUC-CQMU-2023-0137).

Analysis of Virological Indicator Levels

During the treatment period, mice underwent blood collection every Sunday via the orbital sinus. Serum samples were obtained and utilized to measure HBsAg and HBeAg levels employing ELISA kits in strict adherence to the manufacturer's instructions. Additionally, serum and hepatic HBV DNA levels were assessed utilizing the PCR-fluorescent probe method.

Histological and Immunohistochemical (IHC) Assays

Liver specimens were meticulously fixed in 10% neutral-buffered formalin for a minimum duration of 24 hours before undergoing processing for histological scrutiny. Subsequently, paraffin-embedded samples were meticulously sectioned at approximately 5 μm thickness and subjected to staining with hematoxylin and eosin (HE) to elucidate tissue morphology. IHC staining of paraffin-embedded tissue was employed to evaluate hepatic HBcAg and HBsAg expression.

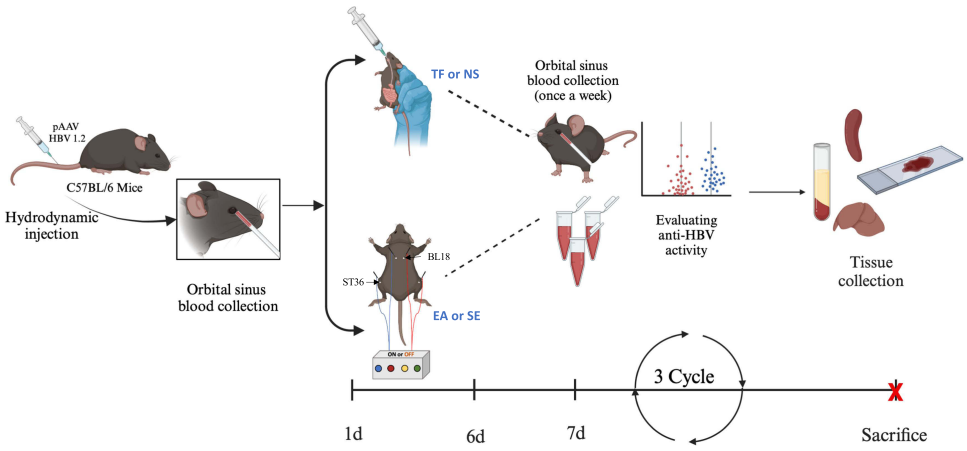

Figure 1 The flow chart of the animal experiment.
Abbreviations: TF, tenofovir disoproxil fumarate; NS, normal saline; EA, electroacupuncture; SE, sham EA.

Transcriptomics Analysis

Fresh liver tissue samples obtained from mice were promptly collected, and total RNA extraction was performed utilizing the Trizol kit. Subsequently, mRNA was enriched using Oligo (dT) beads. The enriched mRNA was subjected to fragmentation into shorter fragments employing a fragmentation buffer, followed by reverse transcription into complementary DNA (cDNA). The purified double-stranded cDNA fragments underwent end-repair, addition of an "A" base, ligation, and subsequent purification. Further purification of the ligated fragments was accomplished using AMPure XP beads. The ligated fragments were then size-selected via agarose gel electrophoresis and then amplified by PCR. The resulting cDNA library was subjected to sequencing by Gene Denovo Biotechnology Co. (Guangzhou, China) utilizing the Illumina Novaseq 6000.

Non-Targeted Metabolome Analysis

Sample Preparation

150 mg of mouse feces were added to 600 μL of methanol containing 2-chlorophenylalanine and subjected to vortex oscillation. Subsequently, steel beads were added for grinding (50 hz, 120 s), followed by ultrasonic treatment. The samples were then centrifuged at 12,000 rpm for 10 minutes, and the supernatant was collected and filtered through a 0.22 μm membrane filter. The filtrate was collected for analysis.

Liquid Chromatography Conditions

The LC analysis was conducted using an ACQUITY UPLC System (Waters, Milford, MA, USA). Chromatography was carried out with an ACQUITY UPLC ® HSS T3 (100 × 2.1 mm, 1.8 μm) (Waters, Milford, MA, USA), maintained at 40°C. The flow rate and injection volume were set at 0.3 mL/min and 2 μL, respectively. Chromatographic conditions for LC-ESI (+)-MS and LC-ESI (-)-MS are provided in Supplementary Tables 1 and 2.

Mass Spectrum Conditions

Metabolite detection was carried out using the Q Exactive mass spectrometer (Thermo Fisher Scientific, USA) equipped with an ESI ion source. The analysis employed simultaneous MS1 and MS/MS acquisition in Full MS-ddMS2 mode with data-dependent MS/MS. Instrumental parameters included sheath gas pressure (40 arb), auxiliary gas flow (10 arb), spray voltage (3.50 kV for ESI(+) and −2.50 kV for ESI(-), capillary temperature (325°C), MS1 range (m/z 100–1000), MS1 resolving power (70000 FWHM), 3 data-dependent scans per cycle, MS/MS resolving power (17500 FWHM), normalized collision energy (30 eV), and automatic dynamic exclusion time.

Flow Cytometric Analysis

The impact of EA on the quantity and functionality of mouse spleen T cells was assessed via flow cytometry assay. T cells were isolated from mouse spleens by grinding and lysing erythrocytes. Membrane molecules including CD3, CD4, CD8, CD69, as well as intracellular markers IFN-γ and TNF-α within T cells, were visualized using fluorescently labeled antibodies and analyzed on CytoFLEX flow cytometer (Beckman Coulter). The acquired data were statistically analyzed using FlowJo v10.

Western Blotting

Liver tissue (50 mg) was homogenized in 1 mL of RIPA lysate containing a protease inhibitor at a frequency of 100 hz for 90 seconds, and the supernatant was collected. Protein concentrations were quantified using the enzyme-labeled instrument. The collected proteins were separated by sodium dodecyl sulfate-polyacrylamide gel electrophoresis and transferred to a polyvinylidene fluoride membrane, which was subsequently blocked with 5% skimmed milk for 1 hour. Following blocking, the membrane was incubated with primary antibodies targeting JAK1 (1:1000), p-JAK1 (1:1000), JAK2 (1:1000), p-JAK2 (1:1000), SOCS-1 (1:1000), STAT1 (1:1000), p-STAT1 (1:1000), IRF8 (1:1000), and β-Tubulin (1:10,000), with β-Tubulin serving as the loading control. After primary antibody incubation, the membrane was probed with the appropriate linked horseradish peroxidase secondary antibody, and bands were visualized using an enhanced chemiluminescence detection reagent and developed on film.

qRT-PCR

Liver tissue total RNA was extracted utilizing the TRIzol reagent following the manufacturer's protocol. Subsequently, the extracted RNA was reverse transcribed into cDNA using the RT Master. Real-time PCR was conducted using the SYBR Green qPCR Master Mix kit. Specific primer sequences designed and employed for real-time PCR are detailed in Supplementary Table 3. The expression of related genes was calculated by $2^{-\Delta\Delta CT}$ relative to GAPDH.

Immunofluorescence (IF)

After dewaxing, the paraffin sections underwent repair, permeabilization, and blocking procedures. Subsequently, the sections were incubated overnight at 4°C with primary antibodies targeting p-JAK1 (1:100), p-JAK2 (1:100), SOCS-1 (1:100), p-STAT1 (1:500), and IRF8 (1:200), respectively. Following three washes with PBS, the paraffin sections were incubated with the corresponding secondary antibodies. Nuclei were counterstained with 4',6-Diamidino-2-Phenylindole (DAPI, 1:1000) staining working solution, and images were visualized and captured using an inverted fluorescence microscope.

Data and Statistical Analysis

Statistical analysis was conducted utilizing GraphPad Prism 9 (San Diego, CA, United States) and Microsoft Excel. The data were tested for normality and were found to conform to a normal distribution, presented as mean ± standard deviation ($\overline{x}\pm$ s). The unpaired Student's *t*-test was employed to assess significant differences between two groups, while one-way analysis of variance (ANOVA) was utilized for comparisons involving three or more groups. Statistical significance was defined as a *p*-value less than 0.05, with significance levels denoted as $*p < 0.05$ and $**p < 0.01$.

Results

EA Possesses Antiviral Effects in a Mouse Model of HBV Replication

In a 3-week treatment, significant reductions in serum HBV DNA levels were observed in EA-treated mice, with a decrease of 1.10 $\log_{10}$ IU/mL compared to the NS group. In contrast, SE and TF-treated mice exhibited reductions of 0.19 and 1.98 $\log_{10}$ IU/mL, respectively. Concurrently, hepatic HBV DNA levels decreased by 1.09 $\log_{10}$ IU/mL in EA, 0.24 $\log_{10}$ IU/mL in SE, and 2.03 $\log_{10}$ IU/mL in TF, all relative to the NS group. Notably, the EA treatment resulted in substantial reductions in serum HBeAg levels, with a decrease of 43.86%, compared to reductions of 8.74% and 8.03% in the SE and TF groups, respectively. Similarly, reductions in serum HBsAg levels were observed, with reductions of 28.01%, 0.26%, and 9.39% noted in EA, SE, and TF-treated mice, respectively (Figure 2A–D). Importantly, measurements of liver function revealed no significant differences in serum AST and ALT between groups, indicating that EA did not induce liver damage (Figure 2E and F). Furthermore, histopathological examination of liver tissues showed no significant pathological differences among the groups, confirming the absence of EA-induced liver toxicity (Figure 2G). Additionally, IHC results further demonstrated significant inhibition of HBsAg and HBcAg expression in the liver tissues of EA-treated mice compared to the NS, SE, and TF group (Figure 2H and I). These observations imply that EA can effectively inhibit HBV DNA and antigens without compromising liver function.

EA Enhances Immune-Related Transcriptional Profiles in HBV-Infected Mice

To delve deeper into the molecular mechanisms underlying the antiviral effects of EA, transcriptomic sequencing was conducted. Differential expression gene (DEG) screening based on criteria of $|\log2\ \text{FoldChange}| > 1$ and $p < 0.05$ revealed 620 DEGs in the livers of EA-treated mice, comprising 331 up-regulated genes and 289 down-regulated genes compared to the NS (Figure 3A–E, Supplementary Table 4). Gene ontology (GO) analysis unveiled significant enrichment of terms associated with key immunomodulatory functions, including nucleotide binding, nucleoside phosphate binding, and 2'-5'-oligoadenylate synthetase activity (Figure 3F–H). Additionally, the Kyoto Encyclopedia of Genes and Genomes (KEGG) enrichment analysis demonstrated significant enrichment of immune-related pathways such as Nod-like receptor, Th17 cell differentiation, and Th1 and Th2 cell differentiation (Figure 3I). Moreover, KO analysis of Th1 and Th2 cell differentiation revealed a close association with IFN-γ (Figure 3J). Transcription factor prediction results

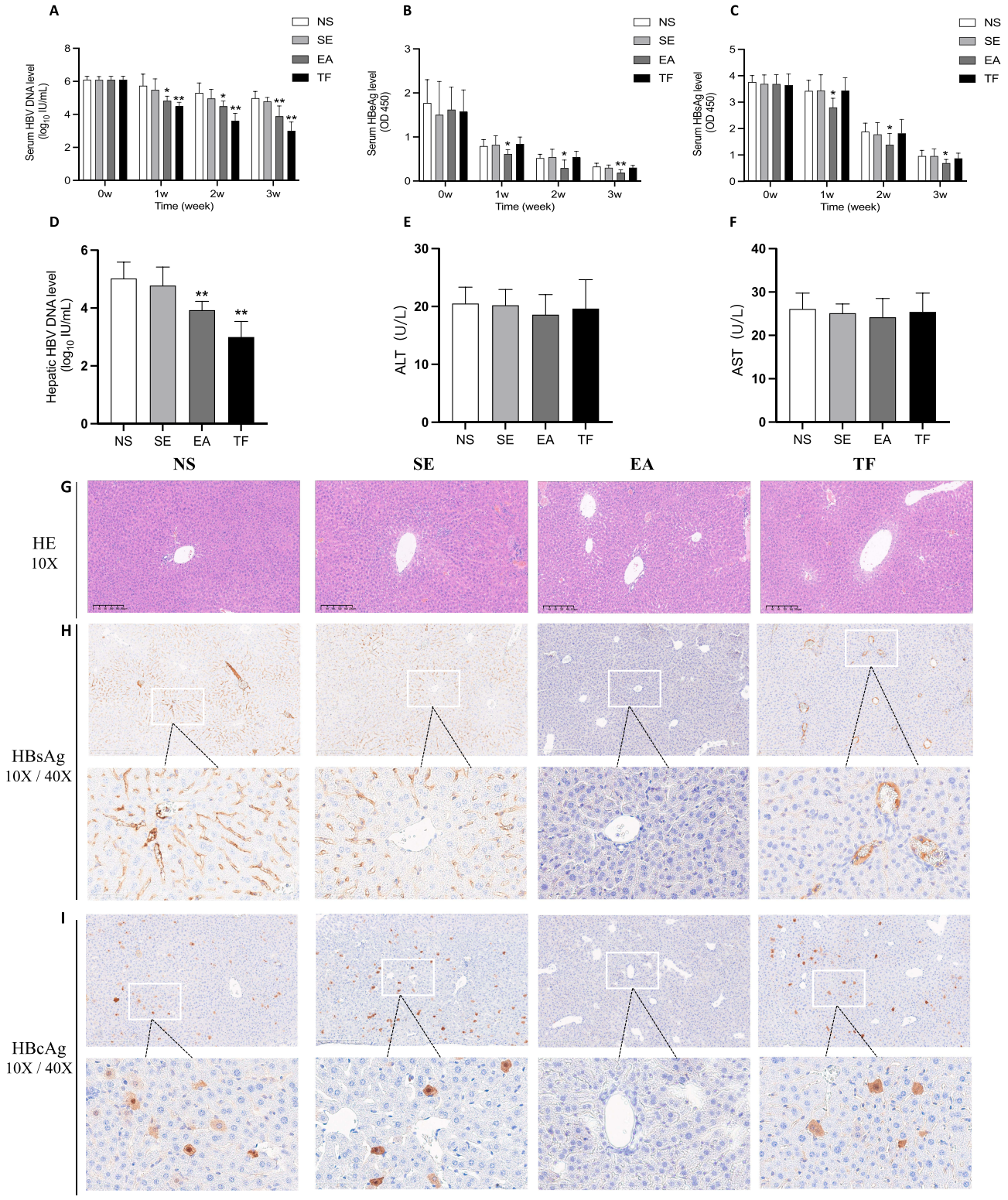

Figure 2 The antiviral effects of EA were evaluated.

Notes: (**A-C**) illustrate the levels of HBV DNA, HBeAg, and HBsAg in serum weekly, while (**D-F**) display the hepatic HBV DNA and serum ALT and AST levels. (**G**) exhibits hematoxylin and eosin staining of the liver tissue, while (**H** and **I**) represent the HBsAg and HBcAg immunohistochemical staining of the liver tissues, respectively. *$p<0.05$, **$p<0.01$ compared to the NS.

Abbreviations: NS, normal saline; TF, tenofovir disoproxil fumarate; EA, electroacupuncture; SE, sham EA.

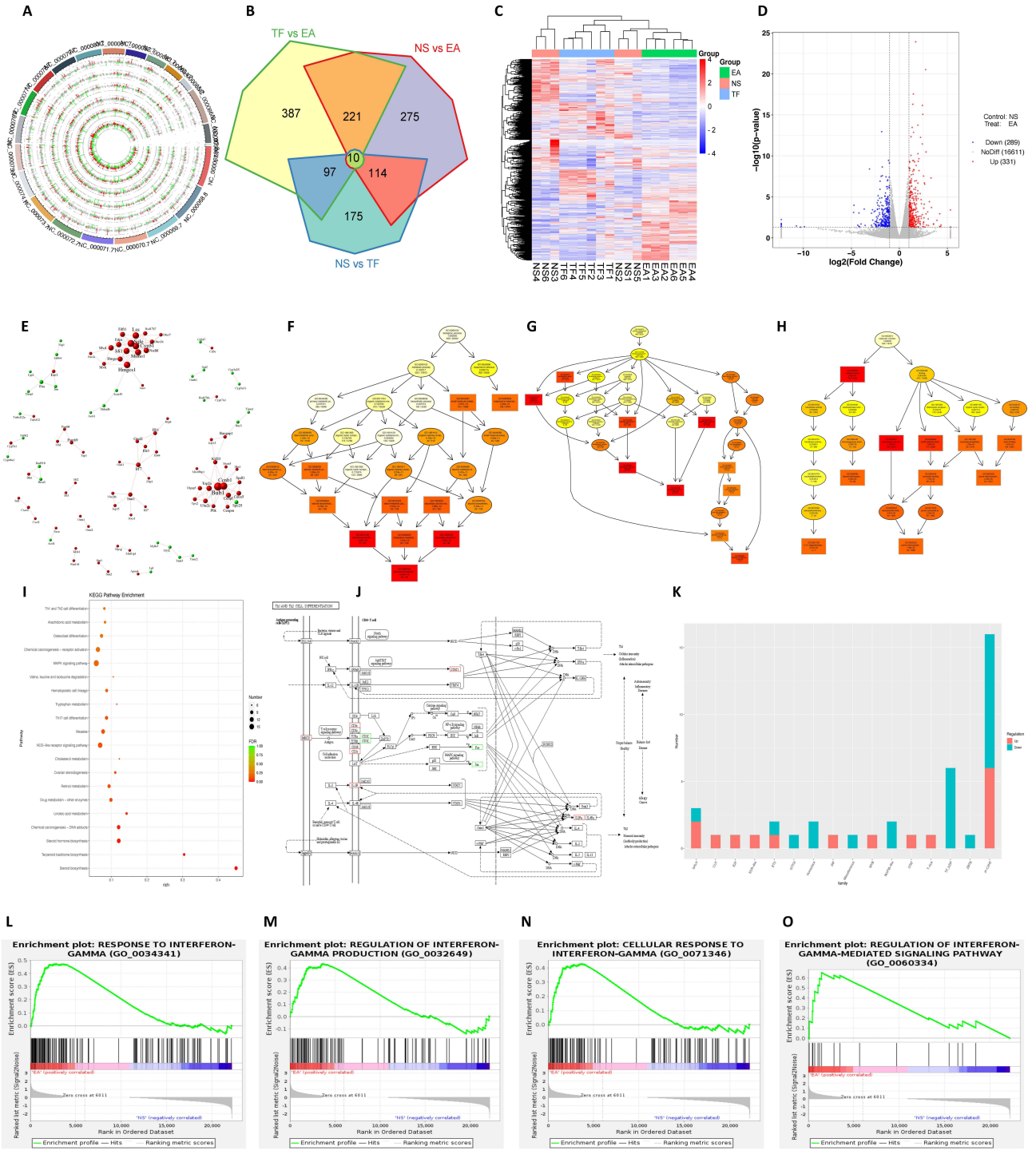

Figure 3 Analysis of target and pathway of EA against HBV based on transcriptomics.

Notes: (**A**) shows Genome circle diagram, where the outermost circle represents chromosome stripes, followed by the results of a differential expression analysis for various comparative groups. Red, green, and gray denote up-regulated, down-regulated, and non-differentially expressed genes (DEGs), respectively. (**B**) demonstrates a Venn diagram illustrating the number of DEGs among the three groups (NS vs EA, NS vs TF, and TF vs EA), as well as the overlapping relationships among the comparative groups. (**C**) depicts a clustering diagram of DEGs, with red denoting up-regulation, and blue indicating down-regulation. (**D**) presents DEGs of NS vs EA, where red, green, and gray represent up-regulated, down-regulated, and non-DEGs, respectively. (**E**) illustrates protein network interaction analysis showing DEGs of NS vs EA. (**F-H**) display the results of GO (Gene Ontology) enrichment of DEGs of NS vs EA, focusing on BP (Biological Process), CC (Cellular Component), and MF (Molecular Function), with darker colors representing a higher degree of enrichment. (**I**) exhibits KEGG (Kyoto Encyclopedia of Genes and Genomes) enrichment results of NS vs EA DEGs. (**J**) demonstrates KO analysis of Th1 and Th2 cell differentiation. (**K**) provides NS vs EA differential transcription factor analysis. (**L-O**) showcase IFN-γ-related GSEA analysis.

Abbreviation: NS, normal saline; TF, tenofovir disoproxil fumarate; EA, electroacupuncture.

indicated significant upregulation of signal transducer and activator of transcription (STAT) and interferon regulatory factor (IRF) genes (Figure 3K). Furthermore, Gene Set Enrichment Analysis (GSEA) highlighted that the expression pattern of genes involved in the IFN-γ functional pathway closely resembled that of the EA group, suggesting activation of the IFN-γ functional pathway in the EA-treated mice (Figure 3L–O). Overall, these findings suggest that EA treatment significantly alters transcriptional profiles in HBV-infected mice, with a particular emphasis on the modulation of immune-related genes and pathways, especially those involving IFN-γ and its associated signaling mechanisms.

EA Enhances Taurine Metabolism in HBV-Infected Mice

To further elucidate the altered metabolic pathways associated with EA against HBV, fecal metabolites underwent analysis using a non-target metabolomics approach. Principal Component Analysis (PCA) coupled with Orthogonal Partial Least Squares Discriminant Analysis (OPLS-DA) revealed distinct differences in the metabolic profiles among the NS, TF, and EA groups (Figure 4A–D). Differential metabolites were screened based on the criteria of VIP > 1 and $p < 0.05$. A total of 47 and 81 differential metabolites were identified and characterized in the TF vs NS and EA vs NS, respectively (Figure 4E–G, Supplementary Tables 5 and 6). Notably, the top five differential metabolites up-regulated in the EA vs NS were guanidinosuccinic acid, L- Rhamnofuranose, taurine, hippuric acid, and tryptophanol (Figure 4H and I). Through KEGG enrichment analysis, immune-related metabolic pathways such as taurine and hypotaurine metabolism, D-Glutamine and D-glutamine metabolism, and Phenylalanine, tyrosine, and tryptophan biosynthesis were significantly enriched (Figure 4J and K). Focusing on the most highly enriched immune-related metabolic pathway, taurine and hypotaurine metabolism, significant changes were observed in three metabolites induced by EA: L-Glutamic acid (AUC = 0.967), Oxoglutaric acid (AUC = 0.857), and taurine (AUC = 1). Notably, the core effect of metabolite taurine exhibited a substantial increase following EA intervention ($p<0.01$) (Figure 4L–Q). These results point to the conclusion that EA may exert its antiviral effects, at least in part, by modulating key metabolic pathways, particularly those related to taurine and hypotaurine metabolism, thereby contributing to an enhanced immune response against HBV.

Association Analysis Reveals Close Relationship Between EA Antiviral Effects and Immunity

By integrating transcriptome and metabolome data, the expression levels of genes and metabolites were analyzed collectively. The top 50 differential mRNAs and differential metabolites, exhibiting correlation coefficients $|r| > 0.8$ and $p < 0.05$, were utilized to construct correlation trend analysis and Canonical Correspondence Analysis (CCA). Results indicated a strong correlation between the differential genes and metabolites (Figure 5A–D). Enzyme-substrate correlation analysis highlighted that differential mRNAs, such as CYP17A1, Asns, and Acot1, along with differential metabolites including 17a-Hydroxypregnenolone, L-Glutamic acid, and Eicosapentaenoic acid, exerted significant impacts on enzymatic reactions (Figure 5E). KEGG enrichment analysis revealed significant enrichment of immunity-related pathways such as Th17 cell differentiation and Th1 and Th2 cell differentiation (Figure 5F). Further focusing on immunity, a clustering heatmap illustrated significant upregulation of Taurine and STAT1 following EA intervention, with correlation analysis demonstrating a positive correlation between the two (Figure 5G and H and H). Subsequently, correlation analysis of up-regulated differential mRNAs and metabolites with virological indicators showed that STAT1 exhibited a correlation with Hepatic HBV DNA ($p < 0.01$), while Taurine displayed a correlation with HBsAg ($p < 0.01$, Figure 5I). Taken together, these findings indicate that the interplay between differential genes and metabolites, particularly taurine and STAT1, may be crucial in mediating the immune-modulatory and antiviral effects of EA.

Effect of EA on Splenic T Cells Activation

The impact of EA intervention on the immunological status of HBV-infected mice was assessed to explore potential anti-HBV mechanisms from an immune cell perspective. Results indicated no discernible change in the proportion of $CD4^+$ and $CD8^+$ T cell subsets among T cells. However, upon further evaluation of the activation levels of these cell subsets unveiled that EA significantly enhanced the proportion of $CD8^+$ $CD69^+$ and $CD8^+$ IFN-γ^+ T cells compared to the NS ($p < 0.05$ or $p < 0.01$), while it did not affect the activation level of $CD4^+$ T cells (Figure 6).

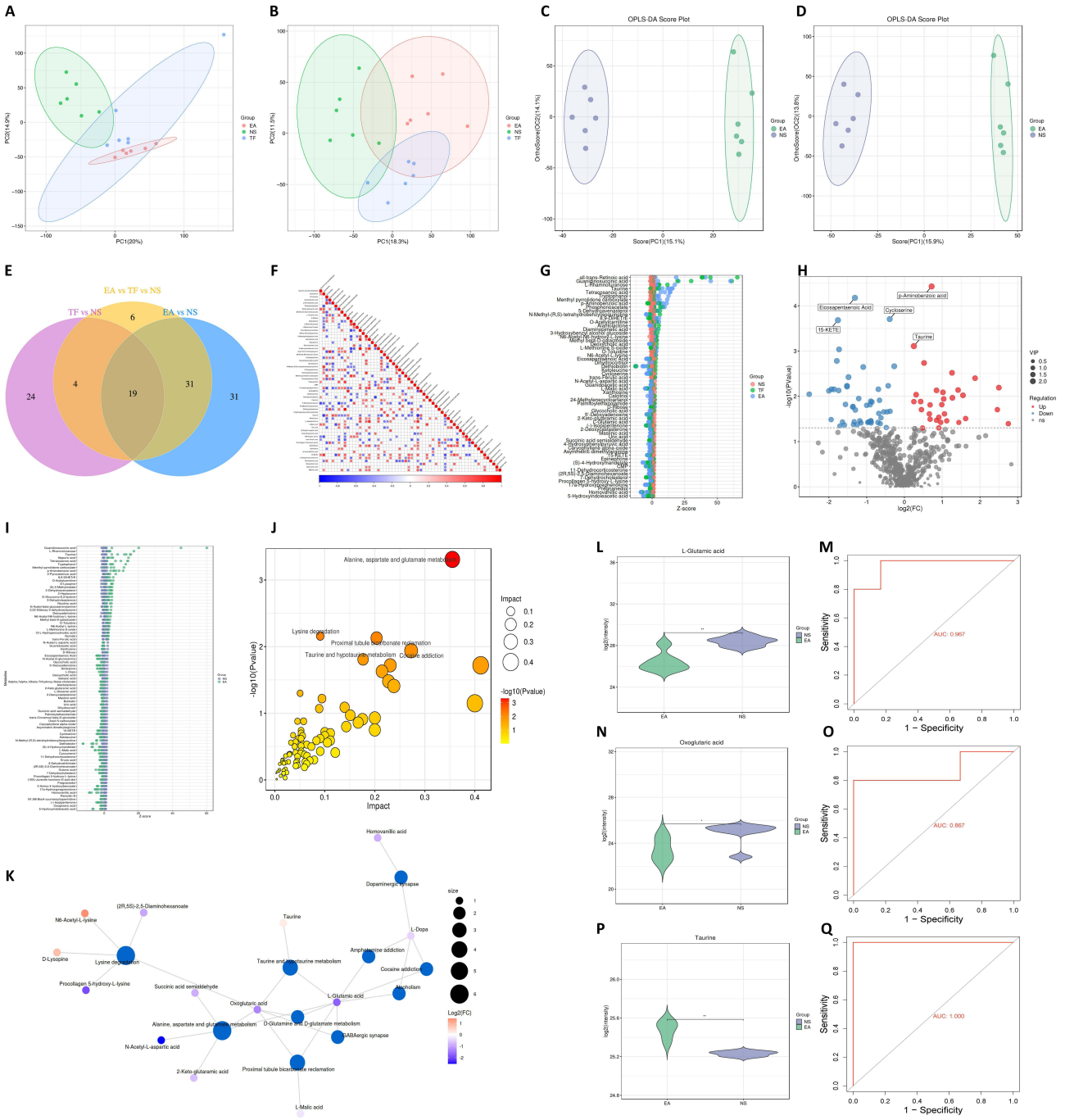

Figure 4 Analysis of target and pathway of EA against HBV based on metabolomics.

Notes: (**A** and **B**) depict Principal Component Analysis (PCA) plots for each group in negative and positive ion modes, respectively. (**C** and **D**) display Orthogonal Partial Least Squares Discriminant Analysis (OPLS-DA) plots comparing NS vs EA in negative and positive ion modes, respectively. (**E**) exhibits Venn diagrams illustrating differential metabolites among NS, EA, and TF. (**F**) shows a correlation heatmap of differential metabolites among NS, EA, and TF, with red indicating positive correlation and blue indicating negative correlation. Darker colors represent stronger correlations. (**G**) presents a Z-score plot of differential metabolites among NS, EA, and TF, points located further to the right indicate higher relative content of metabolites in the group. (**H**) depicts differential metabolites between NS and EA, with red, green, and gray colors representing up-regulated, down-regulated, and non-differential metabolites, respectively. (**I**) illustrates NS vs EA differential metabolite Z-score plot. (**J**) presents NS vs EA differential metabolite KEGG enrichment results, with pathways closer to the upper right corner indicating significant enrichment of differential metabolites. (**K**) displays a network diagram of NS vs EA differential metabolism pathways, where blue represents pathways and other colors represent metabolites, with larger and darker points indicating greater differences. (**L, N, P**) show quantitative results of metabolites, and (**M, O, Q**) represent their ROC results. *p<0.05, **p<0.01 compared to the NS.

Abbreviations: NS, normal saline; TF, tenofovir disoproxil fumarate; EA, electroacupuncture.

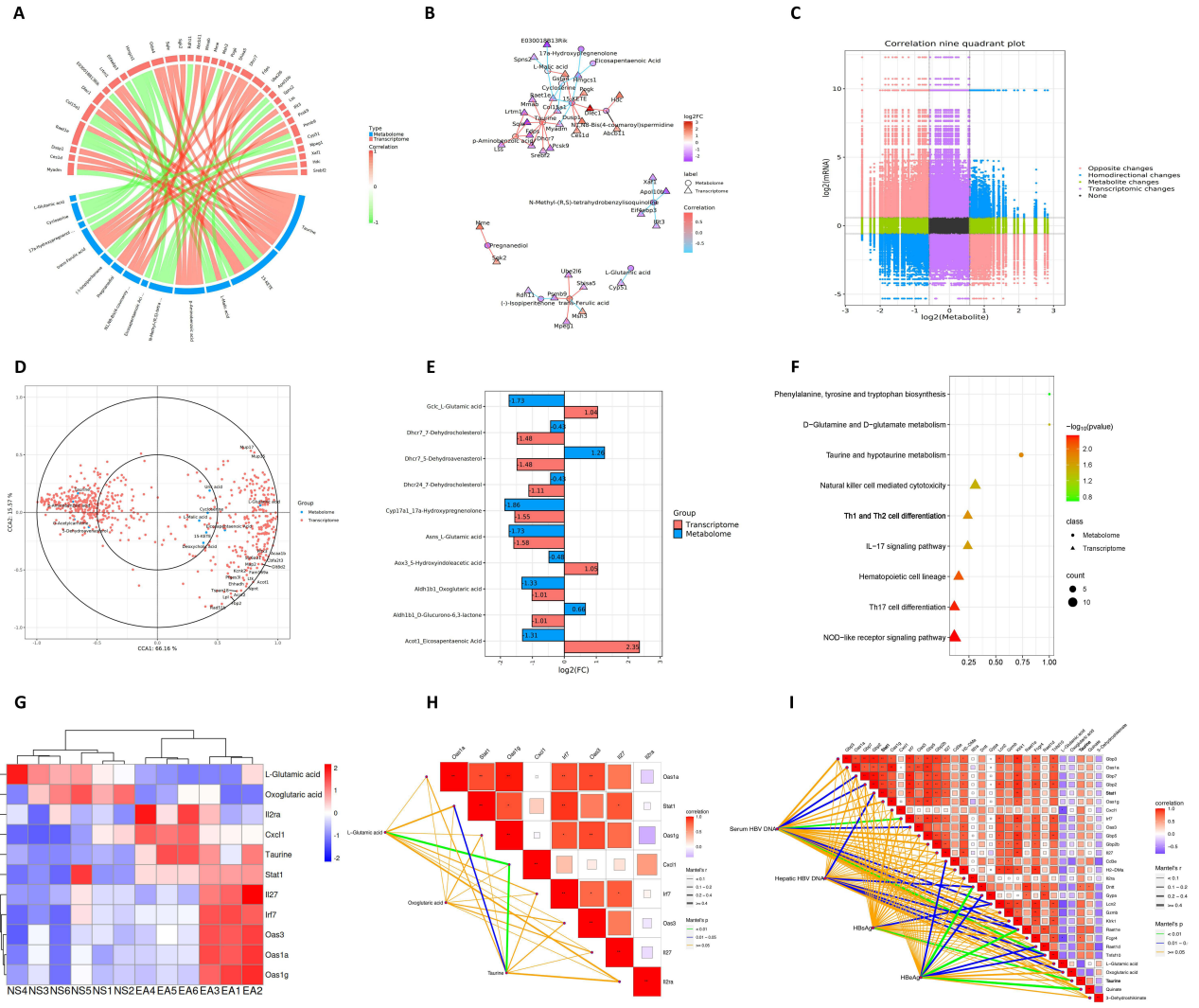

Figure 5 Integrated transcriptome and metabolome analysis.

Notes: (**A**) shows correlation chord diagram, where the red nodes in the upper half represent differential mRNAs, the blue nodes in the lower half represent differential metabolites, and the lines connecting the nodes indicate the correlation relationship between the two (positive correlation shown in red, negative correlation shown in green). (**B**) demonstrates a correlation network diagram illustrating the correspondence between metabolites and mRNAs. (**C**) presents a correlation quadrant diagram. (**D**) exhibits concentric circle plot of correlation between differential mRNAs and differential metabolites in the same region, with the distance from the origin indicating the degree of correlation (the farther away from the origin, the closer to each other, and the higher the correlation). (**E**) shows a histogram depicting the correspondence between metabolites and enzymes, where the horizontal axis indicates the log2(FC) value in different histologies, and the vertical axis indicates the correspondence between mRNA and metabolite in the process of enzyme reaction. (**F**) displays the results of KEGG enrichment analysis of up-regulated differential mRNAs and differential metabolites. (**G**) depicts a heatmap clustering immune-related differential mRNAs and differential metabolites. (**H**) demonstrates a Mantel test analysis of immune-related differential mRNAs and differential metabolites. (**I**) provides Mantel test analysis of up-regulated differential mRNAs, differential metabolites, and therapeutic efficacy. *p<0.05, **p<0.01 (Mantel's test).

EA Promotes Antiviral Effects via Activation of the JAK/STAT Pathway

Key proteins involved in the JAK/STAT signaling pathway were assessed using WB and IF. The findings revealed that EA significantly upregulated the expression of p-JAK1, p-JAK2, p-STAT1, and IRF8 ($p < 0.05$ or $p < 0.01$) while notably inhibiting the expression of SOCS-1, a negative feedback regulator ($p < 0.01$) (Figure 7A and B, H–M). Additionally, qPCR analysis demonstrated that EA significantly enhanced the activation of mRNA expression of JAK1, JAK2, STAT1, and IRF8, along with suppressing SOCS-1 mRNA expression ($p < 0.05$ or $p < 0.01$) (Figure 7C–G). Further examination of downstream signaling in the JAK/STAT pathway was conducted. Serological ELISA and liver tissue qPCR results revealed that EA effectively augmented the production of IFN-γ, TNF-α, and IL-12 ($p < 0.05$ or $p < 0.01$) (Figure 7N–T). Moreover, EA significantly enhanced the expression of IFN-γ, IL-12α, TNF-α, CXCL9, CXCL10, and ISG15 mRNA in

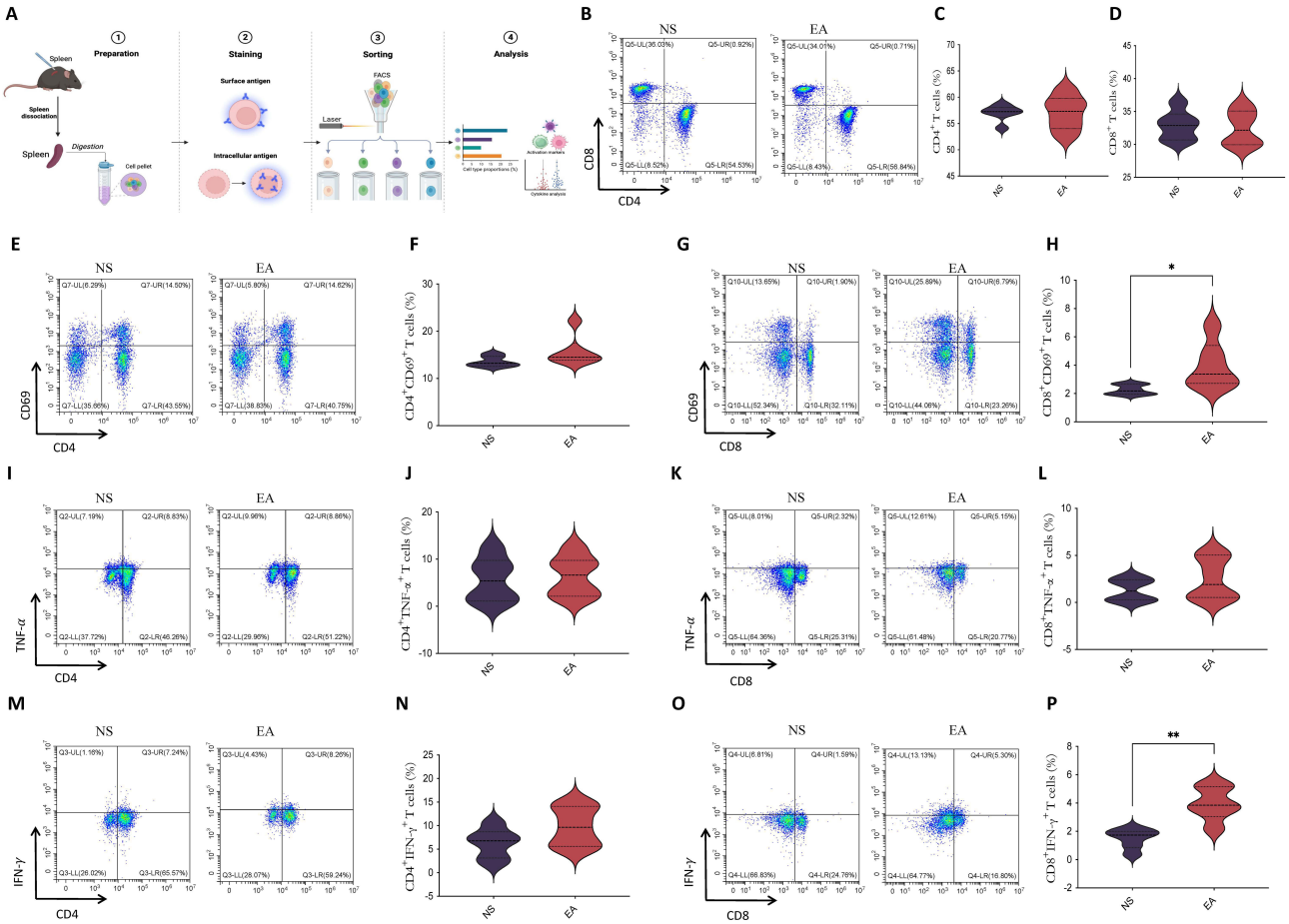

Figure 6 Effect of EA on splenic T cells of HBV-Infected Mice.
Notes: (**A**) shows the flow chart of the flow cytometry experiment. (**B**, **E**, **G**, **I**, **K**, **M**, and **O**) demonstrate the effects of EA on splenic T-cell subsets $CD4^+$ $CD8^+$, $CD4^+$ $CD69^+$, $CD8^+$ $CD69^+$, $CD4^+$ TNF-α^+, $CD8^+$ TNF-α^+, $CD4^+$ IFN-γ^+, and $CD8^+$ IFN-γ^+ expression levels. (**C**, **D**, **F**, **H**, **J**, **L**, **N**, and **P**) represent the results of statistical analysis of the aforementioned cell subpopulations. *p < 0.05, **p < 0.01 compared to the NS.
Abbreviations: NS, normal saline; EA, electroacupuncture.

liver tissue ($p < 0.05$ or $p < 0.01$) (Figure 7O, Q, T-W). In short, these findings underscore EA's role in modulating the JAK/STAT signaling pathway and enhancing downstream immune responses.

Discussion

HBV infection remains a formidable global health obstacle.[13,28,29] Despite the use of prophylactic vaccines for more than four decades and the use of effective viral suppressive drugs since 1998, nearly 300 million people worldwide are still infected with HBV.[2,3] Attaining a functional cure, characterized by antigen negativity, represents the optimal treatment outcome for CHB patients. However, current first-line therapies such as NAs primarily target viral replication and often exhibit limited efficacy in antigen suppression,[30] thus impeding the achievement of functional cure. Acupuncture, a non-pharmacological therapy rooted in traditional Chinese medicine, has demonstrated some efficacy in clinical practice against HBV infection with fewer toxic side effects compared to pharmaceuticals. Nevertheless, modern medical evidence supporting its effectiveness remains scarce. Hence, this study is the first attempt to evaluate the anti-HBV potential of EA and elucidate its antiviral mechanism through basic experimental approaches. The ultimate goal is to offer a viable and complementary therapeutic option for achieving functional cure.

In this study, we established HBV-infected mouse model with intact immune response capability utilizing the high-pressure hydrodynamic method. Subsequently, we assessed the anti-HBV efficacy of EA. Encouragingly, our findings revealed potent antiviral effects of EA, particularly in antigen suppression, surpassing even the efficacy of the positive control TF. Building upon the delineation of these pronounced antiviral effects, our exploration delved into the

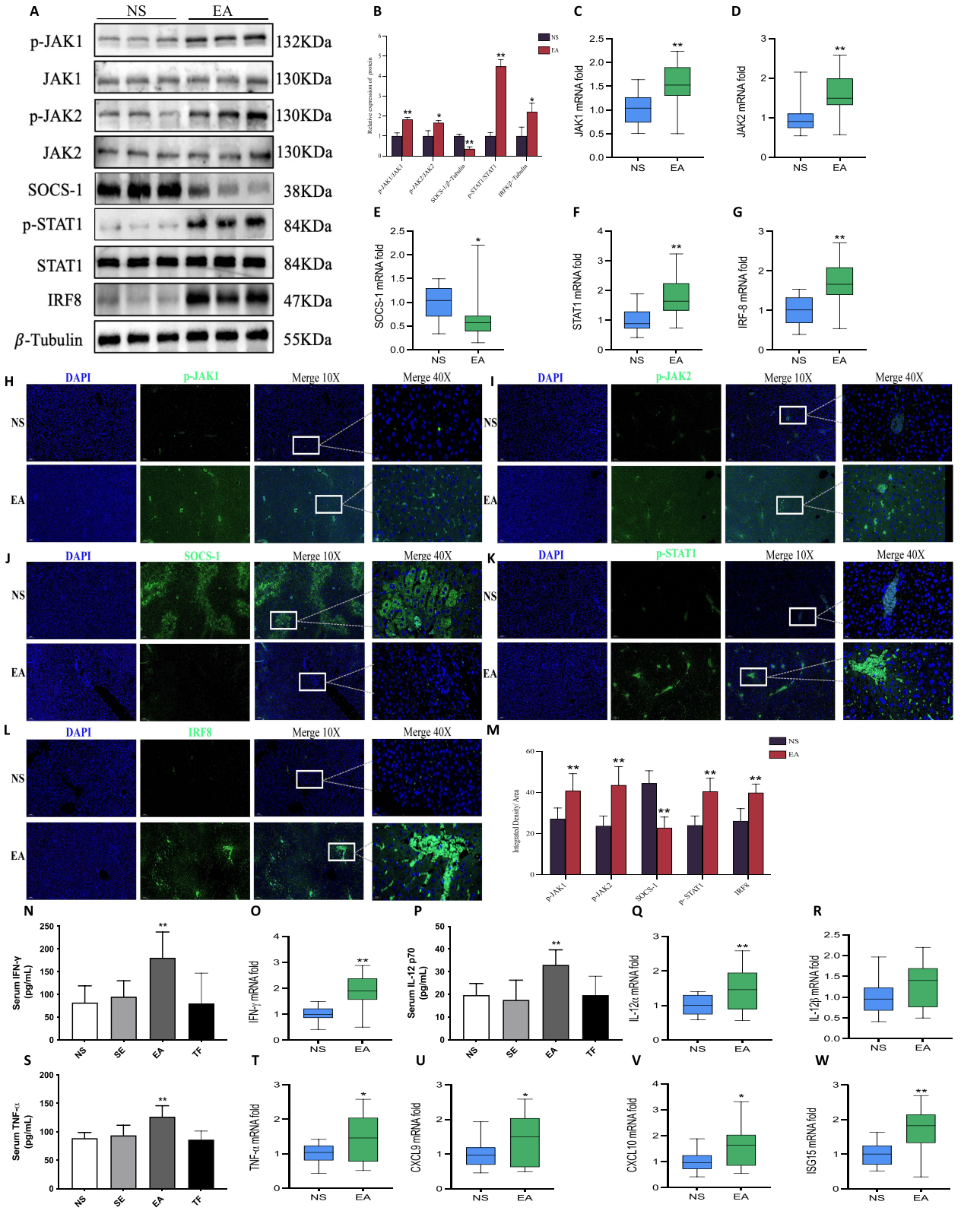

Figure 7 EA promotes the activation of JAK-STAT and downstream signaling.

Notes: (**A**) depicts the Western blot detection of JAK-STAT pathway key protein expression, while (**B**) presents its statistical result. (**C-G**) show qPCR results of mRNA changes. (**H-L**) exhibit immunofluorescence staining results in liver tissues, with (**M**) providing its statistical result. (**N-W**) represent downstream signaling molecules, where (**N**, **P**, and **S**) are serum ELISA results, and the remaining are liver tissue qPCR results. *$p < 0.05$, **$p < 0.01$ compared to the NS.

Abbreviations: NS, normal saline; TF, tenofovir disoproxil fumarate; EA, electroacupuncture; SE, sham EA.

transcriptomic (JAK/STAT) and metabolomic (taurine and hypotaurine metabolism) domains, elucidating the intricate immune-related mechanism underpinning the antiviral action of EA. Subsequent validation via diverse molecular biology experiments confirmed that EA significantly upregulated the expression of pivotal proteins within the JAK/STAT pathway, including p-JAK1, p-JAK2, p-STAT1, and IRF8, while concomitantly suppressing the expression of SOCS-1, a key negative feedback regulator. Furthermore, our comprehensive assessment utilizing flow cytometry, ELISA, and qPCR techniques underscored that EA notably augmented the expression of IFN-γ. In summation, our study delineates a compelling association between the anti-HBV efficacy of EA and the activation of the IFN-γ/JAK/STAT signaling pathway, offering valuable insights into its therapeutic mechanism (Figure 8).

The IFN family comprises cytokines with potent antiviral and immunomodulatory properties, crucial for orchestrating the host's antiviral immune response.[31] IFNs are classified into three types based on their receptor binding specificity: type I (IFN-α, IFN-β), type II (IFN-γ), and type III (IFN-λ).[32] IFN-γ, classified as a type II IFN, is primarily synthesized by various immune cells, including activated T cells, NK cells, macrophages, and natural killer T cells.[33] Its signaling pathway, known as the JAK/STAT pathway, plays a pivotal role in immune-mediated viral clearance. Upon binding to its receptor complex IFNGR1/IFNGR2, IFN-γ activates the JAK1/JAK2 kinases, leading to the phosphorylation and dimerization of STAT1. These activated STAT1 homodimers translocate to the nucleus and bind to gamma-activated sequence (GAS) enhancer elements, initiating transcription of target genes, including interferon-stimulated genes (ISGs) and inflammatory factors. These gene products encode various immune effector molecules, such as chemokines, antigen presentation molecules, and phagocytic receptors, thus exerting potent antiviral effects.[34,35] Of note, IRF8 serves as a pivotal regulator within the type II IFN molecular pathway. It not only influences the secretion of IFN-γ but also modulates the differentiation and function of Th1/Th17 cells and dendritic cells, key players in inflammatory and immune responses.[36] Reduced IRF8 expression has been implicated in various infectious diseases, including CHB, often through activation of the NF-κB signaling pathway.[37,38] In a negative feedback loop, SOCS proteins are upregulated to inhibit the JAK/STAT signaling cascade. They compete with STAT proteins for receptor binding and may facilitate proteasomal degradation of signaling proteins, thereby attenuating the immune response. Our study

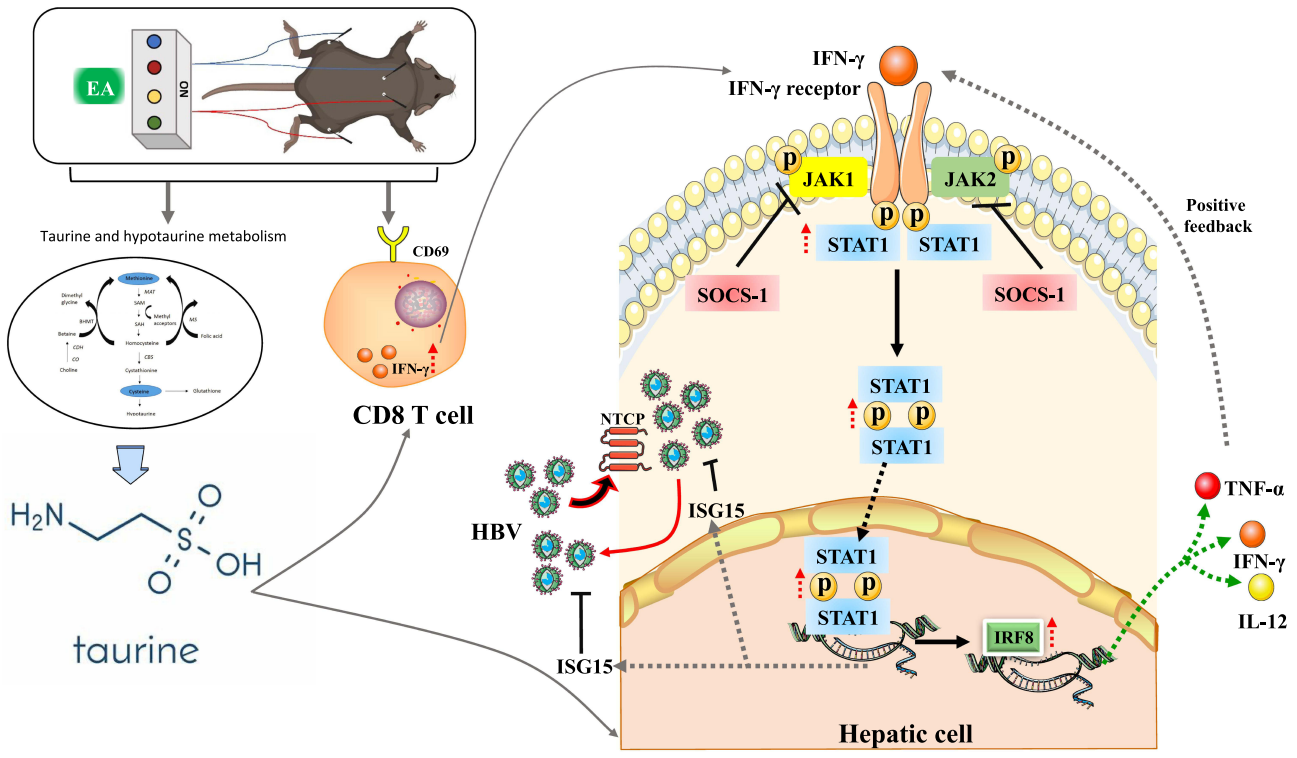

Figure 8 Antiviral effects of EA by modulating the IFN-γ/JAK/STAT pathway against HBV infection.

findings suggest that EA exerts favorable antiviral effects, closely associated with the IFN-γ/JAK/STAT pathway. This elucidates a potential mechanism by which EA modulates the host immune response to combat HBV infection.

Taurine, a vital metabolite in organisms, plays diverse roles, including immune regulation. Our study revealed that EA enhances taurine and hypotaurine metabolism, leading to increased levels of taurine, also known as β-aminoethanesulfonic acid (β-AMES).[39] Taurine, an endogenous sulfur-containing amino acid, possesses various biological functions. Modern research highlights its significance in immunity, fatigue alleviation, nervous system protection, and memory enhancement.[40] In immune regulation, taurine demonstrates the ability to modulate helper T cell subsets, particularly Th1 and Th2 cells. Specifically, taurine has been shown to enhance the activation of Th1 cells, promote Th1 differentiation, and augment Th1-mediated cellular immune responses. Additionally, taurine can stimulate the secretion of Th1-associated cytokines, such as IFN-γ.[41] Considering our study's findings, EA may exert positive regulatory effects on the IFN-γ/JAK/STAT pathway by enhancing taurine expression levels.

The ultimate goal of medical research is to advance clinical development, and this study is no exception. EA, a traditional physical therapy method, continues to play a significant role in modern medicine. Among the key aspects of acupuncture research, including immune regulation, analgesia, and bidirectional modulation, immune regulation stands out as particularly crucial. EA has demonstrated notable efficacy in treating immune disorders like rheumatoid arthritis, chronic inflammatory diseases such as knee osteoarthritis, and chronic neuropathic pain such as back pain, with relatively low side effects.[42,43] Similarly, percutaneous electrical nerve stimulation (PENS), a technique akin to EA, has shown promising results in treating patellar neuropathy, musculoskeletal pain, and diabetic neuropathic pain, demonstrating promising results.[44–46] Our basic research further validates the potential of EA in modulating immune responses and inhibiting HBV infection, providing solid scientific evidence for its clinical application in treating CHB. Clinical evidence also indicates that combining acupuncture with NAs yields superior outcomes compared to using NAs alone. Therefore, in future clinical practice, the combined therapy of NAs and EA should be considered, as this approach may synergistically enhance the antiviral efficacy of NAs, offer a more effective treatment for HBV infection, and ultimately contribute to achieving a functional cure for CHB patients.

Conclusion

In this study, we have discovered that EA effectively suppresses HBV replication in a mouse model, surpassing the inhibitory effect on antigens, particularly HBsAg. Our findings shed light on the underlying mechanism, involving the activation of the IFN-γ/JAK/STAT pathway, leading to heightened production of antiviral effector molecules. These results offer a promising new avenue for the clinical treatment of CHB, particularly in pursuit of functional cure.

Data Sharing Statement

The data will be available from the corresponding author.

Ethics Statement

The animal study was reviewed and approved by committee on the ethics of animal experiments of the Chongqing Medical University (Permit number: IACUC-CQMU-2023-0137).

Consent for Publication

All authors have reviewed the final version of the manuscript and have approved it for publication.

Author Contributions

All authors made a significant contribution to the work reported, whether that is in the conception, study design, execution, acquisition of data, analysis and interpretation, or in all these areas; took part in drafting, revising, or critically reviewing the article; gave final approval of the version to be published; have agreed on the journal to which the article has been submitted; and agree to be accountable for all aspects of the work.

Funding

This study was supported by Chongqing Municipal Health and Family Planning Commission and Chongqing Municipal Science and Technology Commission Jointly Funded Key Research Projects in Traditional Chinese Medicine (ZY201801007), Chongqing Postdoctoral Science Foundation Project (CSTB2022NSCQ-BHX0630), the National funded postdoctoral researcher program of China (GZC20232406), Henan Province Traditional Chinese Medicine Science Research Project (2023ZY3040), Henan Province medical science and technology research plan joint construction project (LHGJ20230233) and the National Natural Science Foundation of China (81930110, 81721002).

Disclosure

The authors declare no conflicts of interest.

References

1. Block TM, Chang KM, Guo JT. Prospects for the global elimination of hepatitis B. *Annu Rev Virol*. 2021;8(1):437–458. doi:10.1146/annurev-virology-091919-062728
2. Jeng WJ, Papatheodoridis GV, Lok ASF. Lok ASF. Hepatitis B. *Lancet*. 2023;401(10381):1039–1052. doi:10.1016/S0140-6736(22)01468-4
3. Hsu YC, Huang DQ, Nguyen MH. Global burden of hepatitis B virus: current status, missed opportunities and a call for action. *Nat Rev Gastroenterol Hepatol*. 2023;20(8):524–537. doi:10.1038/s41575-023-00760-9
4. World Health Organization. Hepatitis B key facts. Available from: https://www.who.int/news-room/fact-sheets/detail/hepatitis-b. Accessed January 21, 2022.
5. Sheena BS, Hiebert L, Han H, GBD 2019. Hepatitis B collaborators. global, regional, and national burden of hepatitis B, 1990-2019: a systematic analysis for the global burden of disease study 2019. *Lancet Gastroenterol Hepatol*. 2022;7(9):796–829. doi:10.1016/S2468-1253(22)00124-8
6. Chinese Society of Hepatology, Chinese Medical Association; Chinese Society of Infectious Diseases, Chinese Medical Association. Guidelines for the prevention and treatment of chronic hepatitis B. *Infect Dis Info*. 2023;36:1–17.
7. Ge F, Yang Y, Bai Z, et al. The role of Traditional Chinese medicine in anti-HBV: background, progress, and challenges. *Chin Med*. 2023;18(1):159. doi:10.1186/s13020-023-00861-2
8. Hsu YC, Jun DW, Peng CY, et al. Effectiveness of entecavir vs tenofovir disoproxil fumarate for functional cure of chronic hepatitis B in an international cohort. *Hepatol Int*. 2022;16(6):1297–1307. doi:10.1007/s12072-022-10411-x
9. Lim SG, Baumert TF, Boni C, et al. The scientific basis of combination therapy for chronic hepatitis B functional cure. *Nat Rev Gastroenterol Hepatol*. 2023;20(4):238–253. doi:10.1038/s41575-022-00724-5
10. Zhao HJ, Hu YF, Han QJ, Zhang J. Innate and adaptive immune escape mechanisms of hepatitis B virus. *World J Gastroenterol*. 2022;28(9):881–896. doi:10.3748/wjg.v28.i9.881
11. Gehring AJ, Protzer U. Targeting innate and adaptive immune responses to cure chronic HBV infection. *Gastroenterology*. 2019;156(2):325–337. doi:10.1053/j.gastro.2018.10.032
12. Cornberg M, Lok AS, Terrault NA, Zoulim F. EASL-AASLD HBV treatment endpoints conference faculty. guidance for design and endpoints of clinical trials in chronic hepatitis B - report from the 2019 EASL-AASLD HBV treatment endpoints conference. *Hepatology*. 2019. doi:10.1002/hep.31030
13. Fung S, Choi HSJ, Gehring A, Janssen HLA. Getting to HBV cure: the promising paths forward. *Hepatology*. 2022;76(1):233–250. doi:10.1002/hep.32314
14. Yardeni D, Ghany MG. Review article: hepatitis B-current and emerging therapies. *Aliment Pharmacol Ther*. 2022;55(7):805–819. doi:10.1111/apt.16828
15. Muñoz-Fernández AC, Barragán-Carballar C, Villafañe JH, et al. A new ultrasound-guided percutaneous electrolysis and exercise treatment in patellar tendinopathy: three case reports. *Front Biosci*. 2021;26(11):1166–1175.
16. Watanabe M, Kainuma E, Tomiyama C. Repetitive manual acupuncture increases markers of innate immunity in mice subjected to restraint stress. *Acupunct Med*. 2015;33(4):312–318. doi:10.1136/acupmed-2014-010660
17. Chen L, Xu A, Yin N, et al. Enhancement of immune cytokines and splenic CD4+ T cells by electroacupuncture at ST36 acupoint of SD rats. *PLoS One*. 2017;12(4):e0175568. doi:10.1371/journal.pone.0175568
18. Kim DJ, Park SH, Seo JC, et al. Efficacy of saam acupuncture treatment on improvement of immune cell numbers in cancer patients: a pilot study. *J Tradit Chin Med*. 2014;34(5):550–554. doi:10.1016/S0254-6272(15)30061-3
19. Hideaki W, Tatsuya H, Shogo M, et al. Effect of 100 hz electroacupuncture on salivary immunoglobulin A and the autonomic nervous system. *Acupunct Med*. 2015;33(6):451–456. doi:10.1136/acupmed-2015-010784
20. Li Z, Li MX, Qin YP, Tang W. Electroacupuncture improves cognitive dysfunction in rats with Alzheimer's disease by regulating microglial cells. *Zhen Ci Yan Jiu*. 2023;48(11):1069–1078. doi:10.13702/j.1000-0607.20230333
21. Xie S, Ling X. Regulative effects of auricular acupuncture, moxibustion and Chinese herbs on immunologic function in the D-galactose-induced aging mouse. *J Tradit Chin Med*. 2008;28(2):129–133. doi:10.1016/S0254-6272(08)60031-X
22. Kong Z, Liang N, Yang GL, et al. Acupuncture for chronic hepatitis B. *Cochrane Database Syst Rev*. 2019;8(8):CD013107. doi:10.1002/14651858.CD013107.pub2
23. Zhou J, You J, Lan Q, Yang L, Ni W. Efficacy analysis of entecavir combined with acupuncture in the treatment of chronic hepatitis B. *Chin Prac Med*. 2021;16(12):170–172.
24. Zhang PJ, Guo JZ. Analysis of HBV patients treated with acupuncture therapy and western medicine treatment. *J LNUTCM*. 2014;16(4):107–108.
25. Yang Y, Ge FL, Deng JY, Yang YH, Luo C, Tang CL. Data mining-based analysis of acupoint selection patterns for chronic hepatitis B infection. *Gastroenterol Hepatol Res*. 2023;5(4):17. doi:10.53388/ghr2023-03-081

26. Guo Y. *Experimental Acupuncture*. Chinese Press of Traditional Chinese Medicine; 2021.
27. Zhang Y, Huang L, Kozlov SA, Rubini P, Tang Y, Illes P. Acupuncture alleviates acid- and purine-induced pain in rodents. *Br J Pharmacol*. 2020;177(1):77–92. doi:10.1111/bph.14847
28. Nguyen MH, Wong G, Gane E, Kao JH, Dusheiko G. Hepatitis B virus: advances in prevention, diagnosis, and therapy. *Clin Microbiol Rev*. 2020;33(2):e00046–19. doi:10.1128/CMR.00046-19
29. Iannacone M, Guidotti LG. Immunobiology and pathogenesis of hepatitis B virus infection. *Nat Rev Immunol*. 2022;22(1):19–32. doi:10.1038/s41577-021-00549-4
30. Yardeni D, Chang KM, Ghany MG. Current best practice in hepatitis B management and understanding long-term prospects for cure. *Gastroenterology*. 2023;164(1):42–60.e6. doi:10.1053/j.gastro.2022.10.008
31. Owen KL, Brockwell NK, Parker BS. JAK-STAT signaling: a double-edged sword of immune regulation and cancer progression. *Cancers*. 2019;11(12):2002. doi:10.3390/cancers11122002
32. Chow KT, Gale M Jr. SnapShot: interferon signaling. *Cell*. 2015;163(7):1808–1808.e1. doi:10.1016/j.cell.2015.12.008
33. Schroder K, Hertzog PJ, Ravasi T, Hume DA. Interferon-gamma: an overview of signals, mechanisms and functions. *J Leukoc Biol*. 2004;75(2):163–189. doi:10.1189/jlb.0603252
34. González-Navajas JM, Lee J, David M, Raz E. Immunomodulatory functions of type I interferons. *Nat Rev Immunol*. 2012;12(2):125–135. doi:10.1038/nri3133
35. Han J, Wu M, Liu Z. Dysregulation in IFN-γ signaling and response: the barricade to tumor immunotherapy. *Front Immunol*. 2023;14:1190333. doi:10.3389/fimmu.2023.1190333
36. Chen M, Wu M, Hu X, et al. Ankylosing spondylitis is associated with aberrant DNA methylation of IFN regulatory factor 8 gene promoter region. *Clin Rheumatol*. 2019;38(8):2161–2169. doi:10.1007/s10067-019-04505-5
37. Yu G, Mu H, Zhou H, et al. MicroRNA-361 suppresses the biological processes of hepatic stellate cells in HBV-relative hepatic fibrosis by NF-kappaB p65. *Cells Dev*. 2021;167:203711. doi:10.1016/j.cdev.2021.203711
38. Zhang X, Yuan S, Zhang X, et al. ANGPTL4 regulates CD163 expression and Kuppfer cell polarization induced cirrhosis via TLR4/NF-κB pathway. *Exp Cell Res*. 2021;405(2):112706. doi:10.1016/j.yexcr.2021.112706
39. You JW, Chen F, Liu Y, et al. Research progress on the efficacy of taurine and its application in the health food. *J Food Safety & Quality*. 2023;14(24):27–34.
40. Jong CJ, Sandal P, Schaffer SW. The role of taurine in mitochondria health: more than just an antioxidant. *Molecules*. 2021;26(16):4913. doi:10.3390/molecules26164913
41. Kong XX, Lan L, Yuan JL, et al. Effect of taurine on the proliferation and differentiation of human peripheral blood T lymphocytes in vitro. *J GXMU*. 2023;40(05):742–748.
42. Vickers AJ, Cronin AM, Maschino AC, et al. Acupuncture trialists' collaboration. acupuncture for chronic pain: individual patient data meta-analysis. *Arch Intern Med*. 2012;172(19):1444–1453. doi:10.1001/archinternmed.2012.3654
43. Chou PC, Chu HY. Clinical efficacy of acupuncture on rheumatoid arthritis and associated mechanisms: a systemic review. *Evid Based Complement Alternat Med*. 2018;2018(1):8596918. doi:10.1155/2018/8596918
44. Martín Pérez SE, Martín Pérez IM, Sánchez-Romero EA, et al. Percutaneous Electrical Nerve Stimulation (PENS) for infrapatellar saphenous neuralgia management in a patient with Myasthenia gravis (MG). *Int J Environ Res Public Health*. 2023;20(3):2617. doi:10.3390/ijerph20032617
45. Plaza-Manzano G, Gómez-Chiguano GF, Cleland JA, Arías-Buría JL, Fernández-de-Las-Peñas C, Navarro-Santana MJ. Effectiveness of percutaneous electrical nerve stimulation for musculoskeletal pain: a systematic review and meta-analysis. *Eur J Pain*. 2020;24(6):1023–1044. doi:10.1002/ejp.1559
46. Hamza MA, White PF, Craig WF, et al. Percutaneous electrical nerve stimulation: a novel analgesic therapy for diabetic neuropathic pain. *Diabetes Care*. 2000;23(3):365–370. doi:10.2337/diacare.23.3.365